Choices for temporal gravity field modeling for precision orbit determination of CryoSat-2

Schrama, Ernst; Visser, P.N.A.M.

DOI
10.1016/j.asr.2023.11.034

Publication date
2023

Document Version
Final published version

Published in
Advances in Space Research

Available online at www.sciencedirect.com

ScienceDirect

Advances in Space Research 73 (2024) 31–41

ADVANCES IN SPACE RESEARCH (a COSPAR publication)

www.elsevier.com/locate/asr

Choices for temporal gravity field modeling for precision orbit determination of CryoSat-2

E.J.O. Schrama *, P.N.A.M. Visser

Delft University of Technology, Faculty of Aerospace Engineering, Kluyverweg 1, 2629HS Delft, the Netherlands

Received 24 July 2023; received in revised form 21 November 2023; accepted 23 November 2023
Available online 27 November 2023

Abstract

In this paper we review the precision orbit determination (POD) performance of the CryoSat-2 mission where we used all tracking data between June-2010 and Jan-2023; with station and beacon coordinates provided in the ITRF2020 reference system, we use a mean gravity model, and we use spacecraft specific models for modeling drag and radiation pressure. To model time variable gravity (TVG) we distinguish between two components, there is a short term oceanic and atmospheric part for which we use the AOD1B model; for the longer term part we employ GRACE and GRACE-FO monthly potential coefficient solutions. Our experience is that adding TVG information is not necessarily successful during POD, and that attention must be paid to the proper processing of the GRACE and GRACE-FO data. To demonstrate this property we define four runs where we gradually implement TVG information. An evaluation criterion is the level of POD tracking residuals, the level of the empirical accelerations, and a comparison to precision orbit ephemeris provided by the Centre National d'Etudes Spatiales (CNES). Unexplained empirical accelerations found during POD are on the level of 3 nm/s^2 for the along-track component and 13 nm/s^2 for the cross-track component. The laser residuals converge at approximately 1.02 cm and the Doppler residuals are on the level of 0.406 mm/s, the radial orbit difference to the CNES POE-F (Precision Orbit Ephemeris version F) orbits narrows to 6.5 mm. Tracking residuals are not evenly distributed for DORIS (Doppler Orbitography and Radiopositioning Integrated by Satellite) beacons, the South Atlantic Anomaly effect is for instance clearly visible in the first empirical orthogonal function EOF mode of monthly binned DORIS residuals. After consideration of all possible TVG approaches our conclusion is that 3 hourly AOD1B model fields result in a small but visible improvement. The addition of TVG from GRACE and GRACE-FO is implemented in two different ways from which we can select a version that does lead to a reduction in the Doppler tracking residuals and which does reduce the level of solved for empirical accelerations.

Keywords: Orbit determination; Temporal gravity modelling; Performance analysis

1. Introduction

The CryoSat-2 mission described in (Wingham et al., 2006) was primarily developed for studying ocean ice thickness whereby use is made of an advanced radar instrument called SIRAL that has synthetic aperture processing capabilities. Other applications of this mission are to study ice sheet topography cf (Khan et al., 2022), also it should be mentioned that the CryoSat-2 mission contributed to observing ocean topography so that the mission contributes to the RADS project, cf (Naeije et al., 2000). The orbit of CryoSat-2 is close to polar and the altitude is approximately 725 km at an inclination of 88 degree. The mission was launched in April 2010, orbit determination is realized with the help of 10s integrated Doppler observations from the international DORIS service cf. (IDS, 2023a) (Willis et al., 2016) and satellite laser ranging obser-

* Corresponding author.
E-mail address: e.j.o.schrama@tudelft.nl (E.J.O. Schrama).

https://doi.org/10.1016/j.asr.2023.11.034
0273-1177/

vations from the international laser ranging service, cf. (ILRS, 2023) (Pearlman and Noll, 2019) and (Noll and Ricklefs, 2019). Tracking of CryoSat-2 is different compared to modern altimeter missions such as Sentinel-6 (Jason-CS) (Donlon et al., 2021) which also carry a Global Navigation Satellite System (GNSS) receiver providing continuous coverage along the orbit. The choice for Doppler and laser tracking was made during the design phase of CryoSat-2 and the result is a situation where we get almost continuous coverage by the IDS network and sporadic laser tracking from the ILRS. POD calculations are divided in arcs with a nominal length of 6 days of which there are 1036 between Jun-2010 and Jan-2023; the arcs are chosen such that we avoid orbit and attitude maneuvers of the spacecraft and that we allow an overlap of approximately 12 to 18 h between the arcs. On average by arc there are 49 Doppler beacons, 1278 passes and 58004 ten second observations, for ILRS there are on average 18 laser tracking stations, 77 passes and 990 range observations by arc.

For CryoSat-2 the consequence of selecting DORIS and laser tracking is that the geometry is less favorable compared to a GNSS receiver on the spacecraft, this can be seen in the station coverage plots shown maintained at (IDS, 2023b) which show that there is no tracking data polewards of latitudes 85°N and 85°S, also there are several open spots in the Pacific ocean and over parts of Antarctica. Maintenance of the DORIS beacon network is a significant task, this activity is documented in the paper by (Saunier, 2023) who mentions that all DORIS beacons need to be visited regularly for maintenance. It also means that local tie vectors to nearby benchmarks and beacons themselves need to be surveyed at regular intervals. A remarkable feature of the DORIS system is that it is self-sustained, by itself it provides all information to model the satellite clock with the help of master beacons that transmit timing pulses synchronized to an atomic time standard. Other processing details are that frequency offsets of the beacons and tropospheric parameters need to be estimated for all beacons seen by the satellite cf. (Schrama, 2018).

The success of a Doppler/laser based approach for CryoSat-2 significantly depends on our ability to perform dynamic orbit determination in a suitable reference system. In this paper we have made a number of assumptions which will be further worked out in Section 2, an important limitation is that we take a single satellite approach with format 2.2 DORIS data and that laser ranging is added to verify the quality of the solution. We review the effect of time variable gravity (TVG) modeling for CryoSat-2 which faces a rich environment of accelerations at an altitude of 725 km. In the end we are able to reach a level of about 1.02 cm in the SLR residuals and 0.406 mm/s for 10 s integrated Doppler data where all tracking data is used between Jun-2010 and Jan-2023. We recognize the fact that the South Atlantic anomaly is affecting the DORIS data, see also (Willis et al., 2004), and present a new method to visualize this effect with the help of empirical orthogonal function (EOF) analysis. We rely on the DPOD2020 reference system, see also (Moreaux et al., 2023), for Doppler beacon coordinates and velocities, DPOD2020 is an update of beacon coordinates and velocities based on the method described by (Moreaux et al., 2019). The contribution of DORIS to ITRF2020 is discussed in (Moreaux et al., 2023). For the laser tracking stations we use ITRF2020 cf. (Altamimi et al., 2023) with the eccentricity vector set made available via (ILRS, 2023).

The implementation of time variable gravity in POD is an actual topic; the paper of (Heike et al., 2022) discusses the benefit of implementing TVG in POD based on GNSS tracking; for DORIS based tracking we find on (IDS, 2023a) a summary how analysis centers (ACs) have implemented time variable gravity in their contribution to ITRF2014. The rationale for considering time variable gravity (TVG) in this paper is to review the status of this topic and to quantify how TVG affects CryoSat-2 POD performance. The TVG model in this paper is based on two sources. **First**, we expect that non-tidal temporal gravity variations originating from oceanic and atmospheric mass changes as contained in the latest release of the AOD1B model cf (Dobslaw et al., 2017) are relevant for POD performance as suggested by (König et al., 2021) for Envisat, Jason-1 and Jason-2. The AOD1B model is based on meteorologic and oceanographic data; the release 6 AOD1B model output is at 3 hourly time steps. AOD1B model output is continuous and we can convert equivalent water height data into spherical harmonics required during POD. **Second**, we expect that TVG which follows from GRACE (Tapley et al., 2004) and GRACE-FO (Kornfeld et al., 2019) monthly potential coefficient data also has an effect on POD. Monthly gravity field variations as obtained from the GRACE mission have been used in (Schrama, 2018). Starting in June 2017 there is a 11 month period without any inter-satellite ranging data until the GRACE follow-on mission returned its first data; in June 2018 the first monthly solutions became available. During this period one can not directly observe TVG changes and one has to rely on an approximation. Also the quality of both space-borne gravimetry datasets is a point of discussion; in (Bandikova et al., 2019) it is explained that an accelerometer replacement procedure is used since October 2016 because only one of the accelerometers was available on GRACE; the same replacement procedure was necessary for the processing of the GRACE-FO data. Based on the GRACE and GRACE-FO data we therefore face the situation where a choice must be made on how to implement the TVG component in the POD procedure. In this paper we will describe two possible scenarios; one where patch functions are estimated with a polynomial procedure, and a second scenario where a Fourier approximation is performed.

The set-up of this paper is as follows, in Section 2 we discuss the assumptions made during POD with emphasis on modeling static gravity, non-tidal ocean and atmo-

sphere time variable gravity and long term TVG from GRACE and GRACE-FO. In Section 3 we will summarize our results based on a number of runs that are defined in Section 2; and in Section 4 we will present our conclusions and recommendations.

2. Method

2.1. Precise orbit determination of CryoSat-2

For this paper we have made use of the GEODYN-II orbit modeling software (Pavlis et al., 2006) with SLR tracking data acquired from the ILRS and 10 s integrated Doppler data from the IDS website, for details see also (Schrama, 2018):

- The nominal orbit computation window (hereafter called arc) lasts 6 days or 144 h; it is chosen in such a way that we stay inside the nominal attitude regime of the satellite which is a four degree yaw steering mode of the AOCS (Attitude Orbit and Control System). Six initial state-vector elements are solved for by arc, the initial guessed state-vector components are interpolated from the DORIS/DIODE navigator orbits provided by the CNES, cf. (Jayles et al., 2015).
- Offset vectors of both the DORIS and the SLR antenna phase centers and their corrections as specified on the IDS website (IDS, 2023a) are taken into account.
- Earth orientation parameters consistent with ITRF 2020 cf. (Altamimi et al., 2023) are taken from the IERS 20 C04 solution as specified in (IERS, 2023a)
- The DORIS beacon coordinates are taken from the DPOD2020 model provided as SINEX files including all updates that have been announced via the IDS during the CryoSat-2 project, coordinates and velocities are taken as in the SINEX files, for newly added DORIS beacons the announced survey values are used.
- SLR station coordinates and their eccentricity vectors are taken from the ILRS SINEX file provided in ITRF2020 cf (IERS, 2023b) while eccentricity vectors are provided by ILRS; no attempt is made to estimate the SLR station coordinates.
- DORIS beacons and SLR stations coordinates are corrected for ocean loading effects whereby use is made of the Chalmers loading calculator (Chalmers, 2023), the reference tide model is FES2014 cf. (Lyard et al., 2021).
- Drag law scaling parameters K_d are estimated every three hours, the thermospheric reference model is based on MSIS 86 cf. (Hedin, 1987); 0.05 square root of variance in the scaling unit of the model are applied to K_d, and continuity constraints are used to connect successive three hourly patch windows, the de-correlation time of the continuity constraints is 1 h.
- A panel model with Lambertian reflection parameters is specified on the International Doris Service (IDS) website cf (IDS, 2023a), we applied a model scaling factor of 1.03 for all arcs; we also used the Earth Albedo model of (Knocke et al., 1988) during orbit determination.
- Measurement biases and tropospheric biases are estimated for all DORIS passes where 10s Doppler data is used for orbit determination; for all laser stations we estimate pass biases within an arc which is recommended for ITRF 2020, cf. (Luceri, 2022).
- The astronomic tide potential and solid Earth tide model involving Love number definitions follows the IERS conventions, cf (Petit and Luzum, 2010). Our earlier POD results were significantly affected by a tide model set-up based on what was used for the EGM96 model (Lemoine et al., 1998). Better results are obtained with a new setup based on the GOT4.7 model which contains ocean tide constants up to degree and order 20 at 31 Doodson lines including air tides constants at 6 Doodson lines. (Richard Ray, personal communication).
- The static gravity model is EIGEN-6S4-V2 (Förste et al., 2016) at reference date 1-Jun-2016, in addition we used three hourly AOD1B model output (Dobslaw et al., 2017) to model the gravitational effect of a barotropic ocean model and atmospheric pressure loading. We use the monthly potential coefficient solutions from the Center of Space Research of the University of Texas at Austin (CSR) release 6 for GRACE and release 6.1 for GRACE-FO with substitutions for $C_{20}$and C_{30} as recommended by (Loomis et al., 2019 and Loomis et al., 2020). The GRACE GRACE-FO TVG model is detailed in Section 2.2.
- Data editing is consistently applied by pass within an arc for all runs. (The definition of a run is that we process all 6 day arcs with the same settings, the definition of a pass is the time period when the satellite is visible from a tracking station). The standard editing procedure is that 3 sigma observation residuals are rejected with a minimum elevation cutoff of 10 degrees. In addition we have applied an a priori observation standard deviation for each DORIS beacon consistent with the residual distributions seen by beacon. The prior observation standard deviation of all SLR stations is set at 3.0 cm.
- All arcs require a number of iterations because the non-linear behavior of the parameter estimation procedure, convergence is usually acquired after three iterations.
- Empirical accelerations are estimated for the along- and cross-track components at the once per orbital revolution frequency including a constant bias term. All empirical acceleration components start with an a priori constraint of 10 nm/s^2. The estimation interval for this parameter group is 6 h where we apply continuity constraints with an a priori standard deviation of 1 $\mu m/s^2$ and a de-correlation time of 1 h. The estimation proce-

dure is repeated twice, in the first iteration we solve all POD parameters, and in the second iteration we apply the updates from the previous step.

2.2. Modeling time variable gravity

We use 218 monthly potential coefficient sets $C(t_k)$ from the CSR release 6 GRACE and release 6.1 GRACE-FO solution available up to Jan-2023, all monthly solutions are complete to degree and order 96 and they are obtained via (PODAAC, 2022). There are various reasons why one can not use $C(t_k)$ directly in a POD procedure, a first reason is that $C(t_k)$ is affected by track noise, a second reason is the presence of data gaps like during the transition between GRACE and GRACE-FO. There are also months where the spherical harmonic solutions are clearly more noisy than usual because both satellites went through an orbital resonance. Our experience is that it is necessary to approximate $C(t_k)$ by a more suitable representation to properly model the GRACE and GRACE-FO TVG effect in POD.

The approximation procedure starts by replacing C_{20} and C_{30} in $C(t_k)$ by values obtained from satellite laser ranging, cf (Loomis et al., 2019 and Loomis et al., 2020). Next we subtract the static gravity field derived from EIGEN-6S4-V2 (Förste et al., 2016) to obtain potential coefficient differences $\delta C(t_k)$. This set is converted into a set of geoid differences $\delta N(t_k)$ at a spatial resolution of one by one degree. During the conversion a block averaging operator of 5.0 degrees is applied cf. (Rapp, 1977). Each element in $\delta N(t_k)$ is reshaped as a column vector in data matrix D which is decomposed in singular values by $D = U\Lambda V^t$ yielding so-called empirical orthogonal functions, cf. (Press et al., 1989). The time representation of each EOF mode provides a handle to isolate anomalous months (Sep-2004 and Feb-2015), furthermore we only used the first 10 modes where all known geophysical signals over the ice sheets and on the continents in $\delta N(t_k)$ appear. EOF compression by editing the Λ matrix on the first 10 modes puts the GRACE and GRACE-FO monthly gravity field information in a form where it can be used for POD applications. After EOF mode compressing and editing we obtain $D^{\star}(t_l)$ which is a set of monthly geoid difference grids at epochs t_l representing all remaining GRACE and GRACE-FO months after editing and represented of the first 10 modes.

A next step is to convert $D^{\star}(t_l)$ into $F(t_m)$ where t_m are all months between Apr-2010 to Jan-2023 for which we make use of patch functions $F(t)$ of which there are two variants based on either a polynomial approximation or a Fourier approximation. The polynomial patch function $F(t)$ with t in decimal years is:

$$F(t) = \sum_{i=0}^{3} p_i (t - t_l)^i \tag{1}$$

where t_l denote epochs in $D^{\star}(t_l)$ within 1 year relative to t, in this case the coefficients p_i are determined such that a least squares minimum is obtained for $F(t_l) - D^{\star}(t_l)$ for each grid element within $D^{\star}$. In a similar way we define for the Fourier patch functions:

$$F(t) = \sum_{i=1}^{2} \{p_i \cos(\omega_i (t - t_l)) + q_i \sin(\omega_i (t - t_l))\} + a_0 + a_1 (t - t_l) \tag{2}$$

where ω_i corresponds to "i" radians per year and where p_i q_i and a_0 and a_1 also follow from the least squares minimum of $F(t) - D^{\star}(t_l)$ for each grid element in $D^{\star}$. The approximation of $F(t)$ is carried out at time steps $t \in t_m$, in the end we get smoothed geoid difference grids with a resolution of 1 by 1 degree which are converted back to spherical harmonic coefficients. The obtained set $\delta C^{\star}(t_m)$ is used during POD by adding spherical harmonic coefficients up to degree and order 40 back to the static gravity field EIGEN-6S4-V2. The last assumption is that we use the nearest element of $\delta C^{\star}(t_m)$ as a constant by arc during POD.

3. Results

To test the success of the TVG model options we define five runs which are detailed in Table 1. This table will serve as a reference for the following subsections which discuss by run type a number of properties such as the residuals of the observations including the geographic representation of the 10 s Doppler data, the level of the empirical accelerations, the correspondence of the along track bias acceleration to F10.7 cm solar flux and the correspondence of empirical accelerations to the β angle of the orbit. We also discuss a comparison of the radial orbit difference to exter-

Table 1
Run definitions, column AOD1B tells whether we use three hourly model output by arc, column TVG reveals whether temporal gravity based on GRACE and GRACE-FO is implemented, details are provided in the comment field. Column tides reveals which set-up was used during POD.

Run	AOD1B	TVG	Tides	Comment
TVG-0	N	N	GOT4.7	No time variable gravity
TVG-A	Y	N	GOT4.7	Only atmosphere and ocean effect
TVG-P	Y	Y	GOT4.7	TVG via polynomial patch model
TVG-F	Y	Y	GOT4.7	TVG via Fourier patch model
TVG-F2	Y	Y	EGM96	TVG via Fourier patch model

nal POE, MOE and NAV orbits provided by the CNES which can be found on the CAL/VAL server of CryoSat, including an assessment of the geographic mapping of the radial orbit differences. The POE orbit of the CNES is according to the GDR-F product agreement of CryoSat, cf (Picot et al., 2018; Couhert, 2017), the MOE orbit is the rapid product available after 1 or 2 days, and the NAV orbit is a real-time product provided by the DORIS/DIODE software on CryoSat-2.

3.1. Residuals of fit

In total there are 1036 arcs nominally 6 days in length between Jun-2010 and Jan-2023, the statistics of the 10 s Doppler and satellite laser ranging residuals are listed in Table 2. The conclusion from Table 2 is that there are small differences between the runs, but that run TVG-A based on only implementing the AOD1B model does help to improve the tracking residuals compared to run TVG-0. At the same time we see that run TVG-P involving the GRACE GRACE-FO model with polynomial approximation increases the laser residuals. Run TVG-F based on the Fourier approximation does improve the Doppler tracking residuals compared to run TVG-A, albeit that the difference is small, also we don't see the improvement in the SLR residuals. Run TVG-F2 is the same as run TVG-F but in this case an old tide-model setup clearly increases all residuals, the only conclusion is that the new GOT4.7 setup is better than what was used for EGM96.

One of the problems with representing tracking statistics as in Table 2 is that SLR and Doppler tracking residuals are represented as averages or medians of standard deviations which follow from a normal distribution. The reality is that tracking residuals are not necessarily normally distributed, an example is demonstrated in (Schrama, 2018) for the South Atlantic Anomaly which is visible in DORIS tracking data residuals for satellites at 725 km such as CryoSat-2. This analysis is extended in Fig. 1 where an

Table 2
Laser residuals and 10 s Doppler residuals statistics, mean and median values refer to the standard deviations obtained for all arcs.

Run	Mean cm	Median cm	Mean mm/s	Median mm/s
TVG-0	1.101	1.036	0.4068	0.4062
TVG-A	1.084	1.014	0.4066	0.4060
TVG-P	1.102	1.033	0.4066	0.4061
TVG-F	1.087	1.020	0.4064	0.4060
TVG-F2	1.280	1.235	0.4100	0.4096

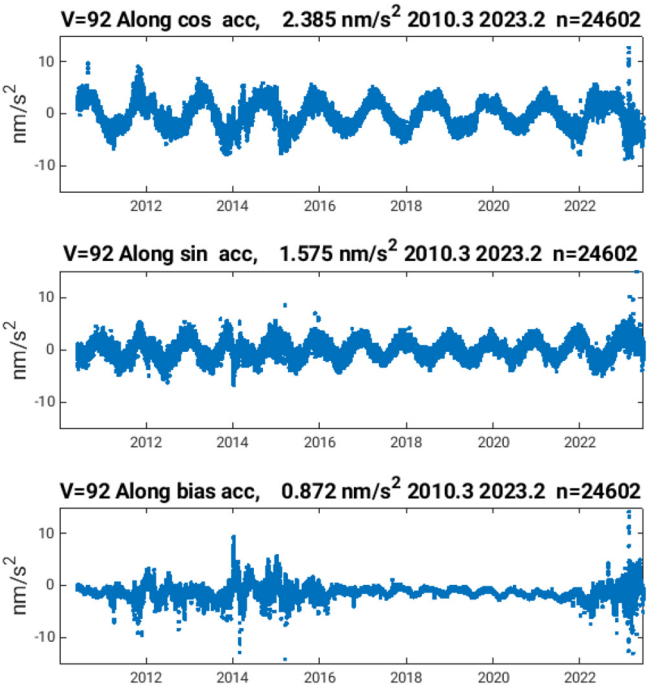

Fig. 2. This figure contains solved for empirical accelerations in the along-track direction, top to bottom cosine, sine and bias. All empirical accelerations are solved for in 6 hourly windows.

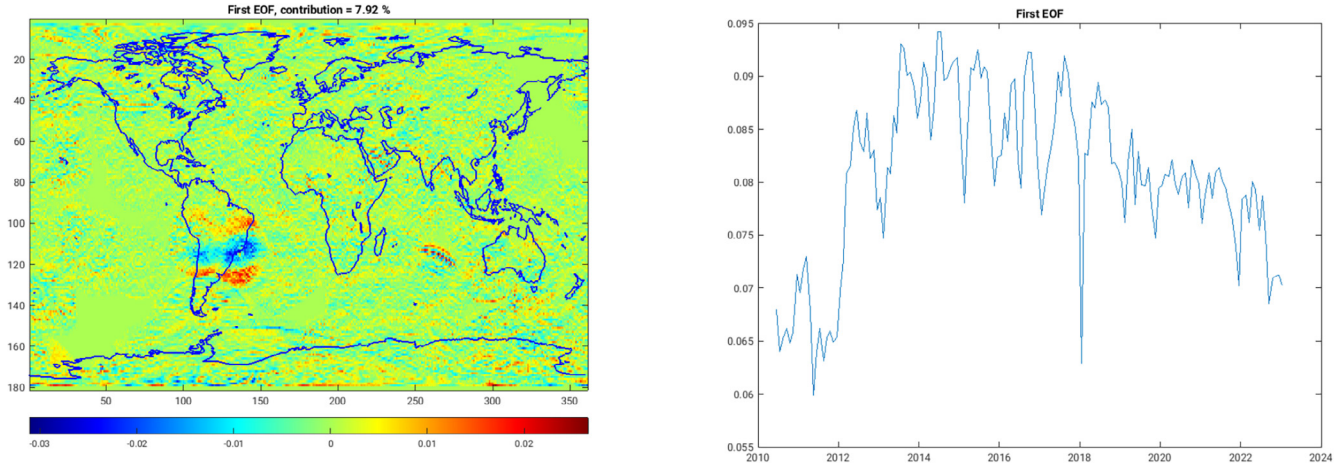

Fig. 1. First mode of the empirical orthogonal function of the DORIS tracking data residuals of run TVG-F. Doppler beacons in the South Atlantic Anomaly region are showing a long term pattern, this mode explains 8% of the total variance.

empirical orthogonal function (EOF) analysis technique is used. In this case the EOFs are obtained from 151 monthly maps where we approximated by grid cell the Doppler residuals, the leading EOF mode of the mapped residuals shows an enigmatic long-term behavior in Fig. 1 which is non-Gaussian.

3.2. Empirical acceleration analysis

During POD we model empirical accelerations for along-track and cross-track components in the local orbit reference frame. The purpose of these parameters is to handle accelerations on the satellite which are not adequately described by the dynamical models. The empirical acceleration model contains cosine and sine terms at the once per orbit frequency including a bias term that are solved for in windows of 6 h by arc. The daily mean of the solved for empirical acceleration components for run TVG-F are shown in Fig. 2 and 3 where a median of the standard deviation of empirical accelerations by arc is found in the figure title. The median value provides an indication of the success of dynamical models applied during POD, details for all runs are summarized in Table 3 where acceleration levels in the columns are labeled as Along, Cross and Total. Based on the total square root of variance of all runs in column "Total" in Table 3 we conclude that the differences are rather small and there is no clear winner. Our preferred solution is however run TVG-F since it yields the lowest total level of empirical acceleration. Run TVG-F2 is no improvement compared to the other runs since EGM96 tide model setup underperforms relative to GOT4.7 set-up.

3.2.1. Along track empirical accelerations at once per orbit

Along-track empirical accelerations as shown in Fig. 4 for the cosine and sine component are correlated to the latitude of the Sun relative to the orbital plane, also known as the β angle. The geometry of the CryoSat-2 orbit is such that β has a periodicity of approximately 460 days. Along track empirical accelerations for the cosine and the sine

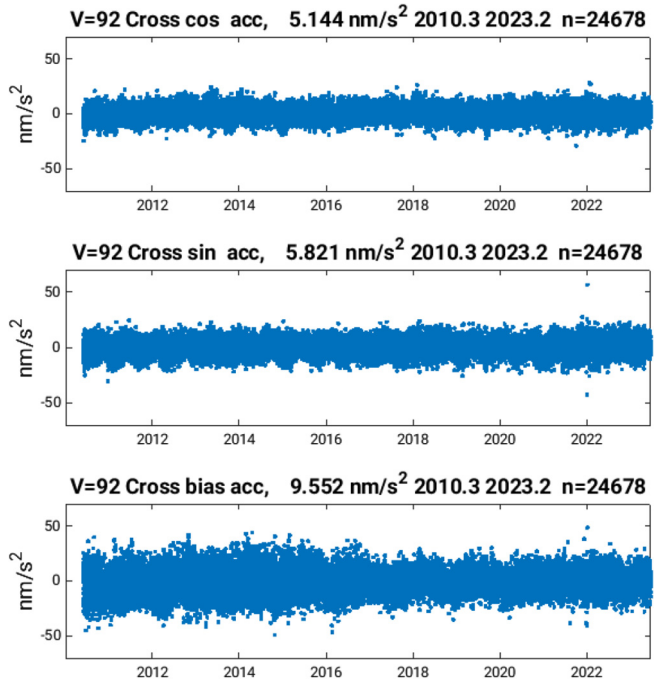

Fig. 3. This figure contains solved for empirical accelerations in the cross-track direction, top to bottom cosine, sine and bias. All empirical accelerations are solved for in 6 hourly windows.

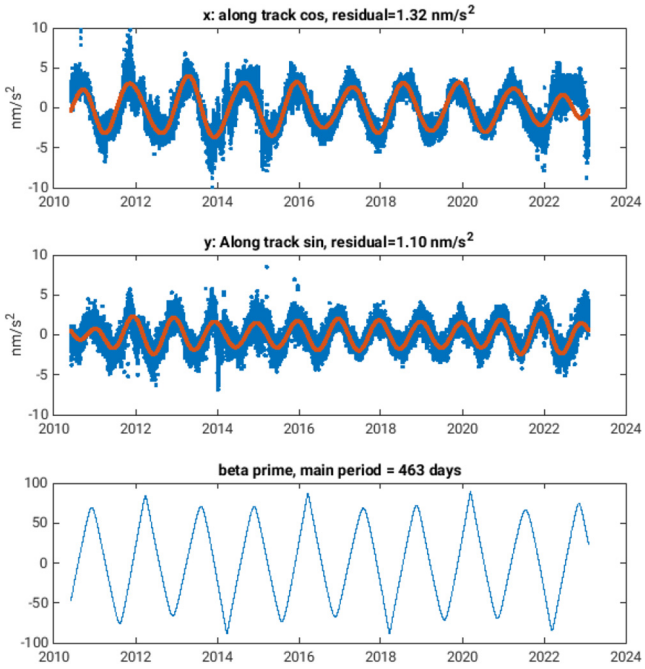

Fig. 4. The top and middle pane show empirical accelerations and the trend functions, the bottom pane shows the evolution of the β angle of the orbit.

Table 3
Columns A_c, A_s and A_b show along track acceleration median standard deviations for cosine, sine and bias parameters respectively, columns C_c, C_s and C_b show similar median standard deviations for the cross-track component, columns "Along" "Cross and "Total" show the acceleration level for each component. Units are in nm/s^2.

Run	A_c	A_s	A_b	C_c	C_s	C_b	Along	Cross	Total
TVG-0	2.53	1.57	0.86	5.32	6.47	9.81	3.09	12.90	13.27
TVG-A	2.42	1.55	0.85	6.03	6.96	10.71	3.00	14.13	14.44
TVG-P	2.37	1.58	0.85	5.39	6.15	9.77	2.98	12.74	13.08
TVG-F	2.36	1.56	0.85	5.14	5.82	9.56	2.95	12.32	12.67
TVG-F2	2.52	1.77	0.87	5.80	6.58	10.12	3.20	13.39	13.77

component can be approximated with a harmonic function with a base period of 463 days modulated by slowly varying harmonic signals with periods up to four years (the total record length is almost 13 years). The estimated functions are shown in red in Fig. 4; both functions are able to capture around 50% of the signal and the residual of fit appears as Gaussian.

Empirical acceleration trend functions as shown could be used as a predictive tool for future arcs in the CryoSat-2 POD activities. An alternative approach could be regular tuning of the scale factor C_r of the solar radiation pressure model by which one could likely obtain the same result. The approach used in this paper relies on the CNES solar radiation pressure model and a one time tuning of the scale factor where we found 1.03. Our current strategy is that we solve for empirical parameters like shown in Fig. 2 and 3 and that we apply the solved for empirical parameters in a second iteration of the arc.

3.2.2. Along track empirical acceleration bias

During POD we solve for a thermospheric drag scaling parameter K_d, for stability reasons this parameter is constrained to 2.2 with an a priori sigma of 0.05. The evolution of solved for K_d values over time shows a Gaussian behavior, there is no dependency to β or annual cycles and no clear relation to the solar flux index. This result contrasts to the behavior of the along-track empirical acceleration bias shown together with the solar flux index obtained from the NOAA Space Weather website (Space Weather Prediction, 2023) in Fig. 5. The variability in the along track empirical bias acceleration clearly correlates to the solar flux index in solar cycle 24 (starting in 2008 and ending in 2019) and the start of solar cycle 25. The solar flux shown in the bottom panel of Fig. 5 was weak between 2017 and 2021 when the F10.7 flux value was often below 80 solar flux units. One SFU is $10^4 \mathrm{Jy} = 10^{-22}\,\mathrm{Wm}^{-2}\mathrm{Hz}^{-1}$, F10.7 flux values are obtained from radiometer measurements at a wavelength of 10.7 cm, or more precisely, a 100 MHz band centered at 2800 MHz, cf (Tapping, 2013). The evolution of the along track bias acceleration shows rapid variations during the peak of solar cycle 24, the acceleration variability reduces between 2017 and 2021 and regains its variability at the start of solar cycle 25. The sun was exceptionally quiet between 2017 and

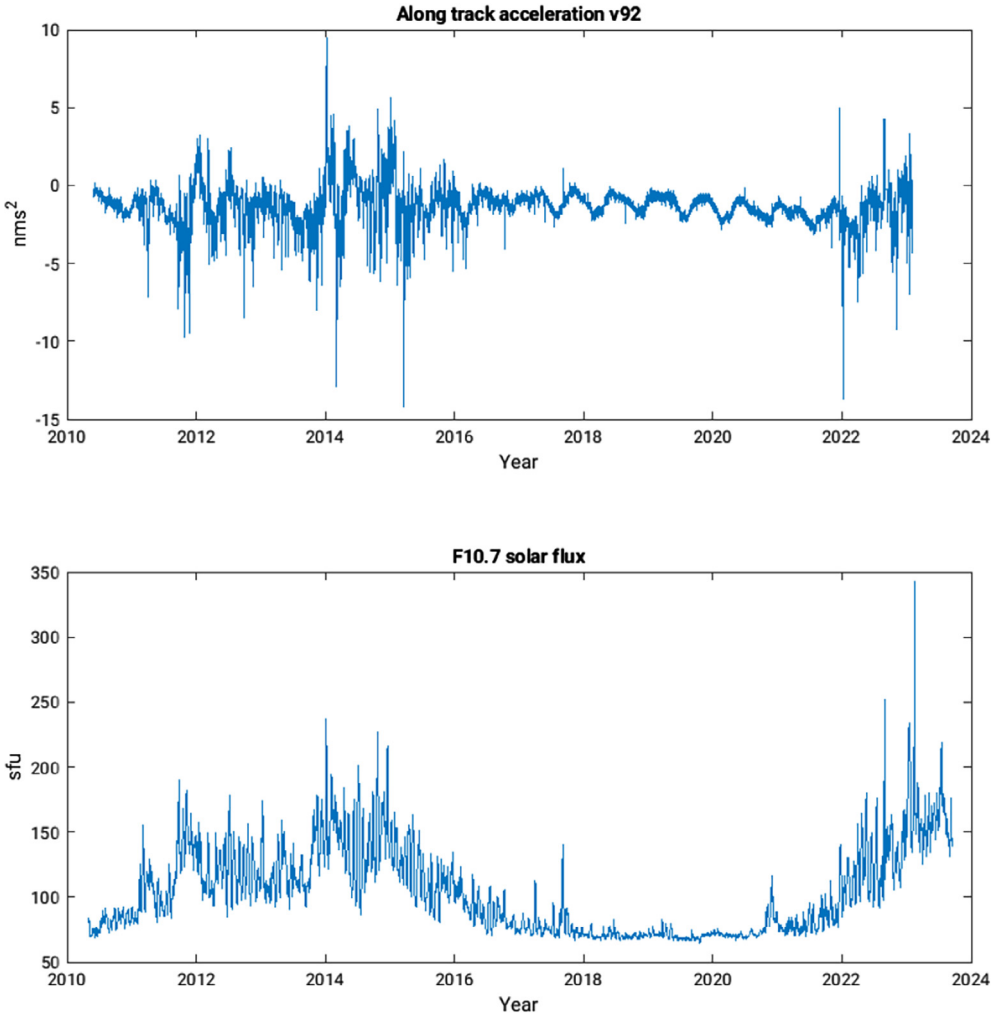

Fig. 5. Top panel: along track bias in nm/s^2 along the CryoSat-2 orbit between Jun-2010 and Jan-2023 for run TVG-F. Bottom panel shows the solar flux at F10.7 where one SFU is equal to 10000 Jansky (Jy).

2021 with SFU values often below 80, this is also the time window where we do not observe large fluctuations in the along track bias acceleration where there is a minor oscillation which is unexplained. The start of solar cycle 25 is in 2019, from this point in time onward we notice more rapid variations in the along track bias accelerations. Our conclusion is that the along track bias variability is caused by the thermospheric reference model to provide densities required for the computation of the drag effect on the satellite. Performance of the thermospheric density model could be discussed if CryoSat-2 were equipped with an accelerometer, calibration of thermospheric models is discussed for instance in (Doornbos, 2012), there are also improved thermospheric models, cf. (Bruinsma and Boniface, 2021 and Emmert et al., 2022) but they were not tested within the scope of this paper.

3.3. Comparison to external orbits

Table 4 and Fig. 6 display radial orbit differences relative to orbit products made available by the CNES. The conclusion is that run TVG-F is closest to the CNES POE-F orbits. (It should be mentioned that the CNES POE-F orbits only depend on DORIS tracking, and that SLR data is used for validation purposes.) The geographic radial orbit differences (computed as an average by grid cell) computed between Apr-2010 and Jan-2023 are shown in Fig. 6 where we can see that the mapped geographic difference is usually smaller than 1 cm. We do notice a typical north–south striping pattern, but we don't notice any hemispherical or tesseral offsets between orbit solutions. Several β cycles are required to obtain the data shown in Fig. 6, in this case we used all available residuals to create the figure.

Table 4
Comparison to external orbits provided by the CNES of the CryoSat-2 project. The (POE) precision orbit is available after 30 days, the (MOE) rapid orbit is available after 24 h, and the (NAV) navigator orbit is computed in real-time by the DIODE Navigator system. The values reported here are in cm as median values by arc, for the navigator orbit we used the navigator solution after the DORIS DIODE software upgrade in the summer of 2012.

Run	NAV	MOE	POE
TVG-0	3.29	0.86	0.73
TVG-A	3.28	0.88	0.68
TVG-P	3.34	0.89	0.69
TVG-F	3.33	0.86	0.65
TVG-F2	3.25	1.31	1.18

3.4. Crossover statistics

Statistics of CryoSat-2 altimeter crossover differences are shown in Table 5, which contains the mean, the root mean square and standard deviations obtained at 670728 data points selected between July 2011 and January 2023, three separate columns in the table show the effect of 3.5 sigma editing. The persistent bias between ascending and descending sea level anomalies at the crossing locations is not related to the used orbit solution, instead it is caused by altimeter time tag errors which in turn depend on the ESA baseline altimeter product that is used in RADS. (Marc Naeije, personal communication). Our selection criteria for crossing track locations is that monthly data batches are used and that a maximal time difference of 13.5 days is allowed at the crossover. We start with 670728 crossover differences where the maximal time difference is 13.5 days, 3.5 sigma editing removes typically 1.5%

Table 5
Crossover Statistics in cm, REF is the CNES POE-F solution on the CryoSat altimeter product. M is the mean at the crossovers, R is the rms and S is the sigma, $M^{\star}$ $R^{\star}$ and $S^{\star}$ are obtained after 3.5 sigma editing.

Solution	M	R	S	$M^{\star}$	$R^{\star}$	$S^{\star}$
REF	−0.79	6.82	6.78	−0.77	5.78	5.72
TVG-0	−0.84	6.87	6.81	−0.83	5.83	5.77
TVG-A	−0.83	6.86	6.81	−0.82	5.82	5.76
TVG-P	−0.68	6.83	6.80	−0.66	5.78	5.75
TVG-F	−0.69	6.82	6.79	−0.66	5.77	5.73
TVG-F2	−0.69	6.98	6.94	−0.66	5.98	5.95

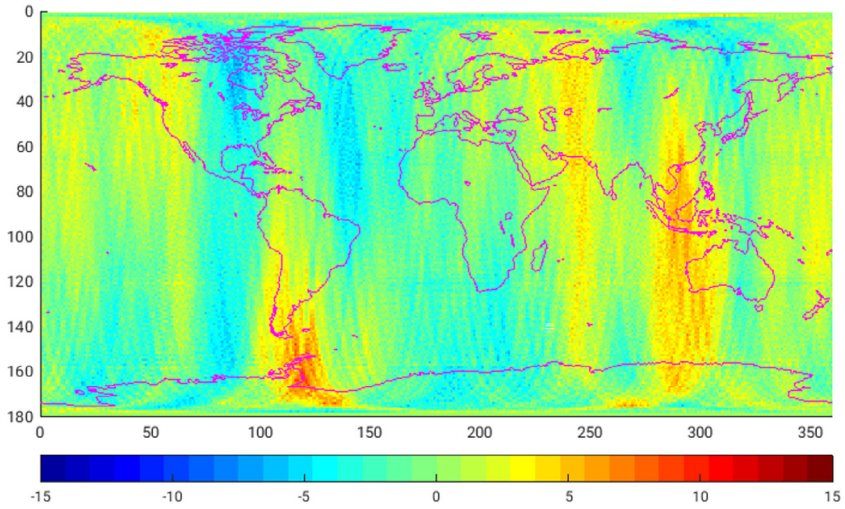

Fig. 6. Radial orbit error difference from run TVG-F relative to the CNES POE-F orbit projected on a map, units: [mm].

of the crossover data typically in regions with high crossover variability.

The benefit of modeling TVG is visible in the crossover differences, i.e. TVG-F is better than TVG-P which is in turn better than a TVG-A model and TVG-0, cf. Table 5. The EGM96 tide model set-up is worse than any of the other setups which are for TVG-0 to TVG-F based on GOT4.7, in the end our TVG-F solution is on a similar noise level compared to the CNES POE-F orbits in RADS.

4. Conclusions

In this paper we focus on the implementation of a time variable gravity (TVG) model that is used for precision orbit determination for CryoSat-2 which is a 92 degree inclination satellite at a height of approximately 725 km tracked by Doppler and satellite laser ranging. Time varying gravity information comes from both GRACE missions, the TVG modeling problem regained attention due to the transition of GRACE to GRACE-FO which not only has caused a data gap of approximately 1 year but also a difference in quality of the available TVG information. In total 5 versions (runs) of the POD implementation were tested, all with a different implementation of the TVG model including an alternative tide model setup. Our control run (TVG-0) does not include TVG effects, run TVG-A only includes AOD1B, run TVG-P is based on AOD1B and a polynomial approximation of TVG from GRACE and GRACE-FO, run TVG-F is based on AOD1B and Fourier approximation of TVG. TVG-F2 is like TVG-F except that an older tide model set-up is used while TVG-0 to TVG-F all rely on the GOT4.7 tide model setup. Several evaluation criteria for comparing the runs are discussed, we inspect the tracking data residuals, empirical accelerations, differences to external orbits provided by the CNES that are obtained from the CryoSat-2 cal/val server and performance of orbit solutions at crossover differences observed by the CryoSat-2 altimeter.

The conclusion of this study is that incorporating both corrections (TVG being the sum of monthly gravity solutions from GRACE and GRACE-FO and AOD1B model output) during POD has a small improvement of the tracking data residuals. The polynomial TVG approximation method is an example where we deteriorate a POD solution, with the Fourier TVG approximation method we are able to find a solution that outperform other runs. The median standard deviation of the 10s Doppler residuals is 0.406 mm/s, for laser residuals we get 1.02 cm, but at the same time it should be remarked that the residuals are strictly seen not normally distributed. An example is the observation residuals for DORIS which show a long term effect in the South Atlantic Anomaly region, we demonstrate this feature with the help of an empirical orthogonal function analysis of the observation residuals mapped on monthly grids.

The variance of the solved for empirical accelerations is somewhat affected when TVG from GRACE and GRACE-FO and AOD1B corrections are implemented during POD, the total acceleration difference between run TVG-0 and TVG-F is less than 1 nm/s^2, the improvement occurs mostly in the cross track acceleration component. The along track empirical acceleration bias is correlated to the F10.7 solar flux index, during the doldrum between solar cycle 24 and 25 when the solar flux values were less than 80 sfu we see that fluctuations in the along track acceleration bias are reduced compared to the peak of cycle 24 and the onset of cycle 25. Our interpretation is that defects in the a priori thermospheric drag implementation are absorbed in the along-track empirical acceleration biases.

When we compare all performed runs to external trajectories available for CryoSat-2 we see that there is an advantage by incorporating a AOD1B model in POD, including a TVG model based on a combination of GRACE and GRACE-FO data is also helpful, there is no indication that the transition gap from GRACE to GRACE-FO significantly affects the POD performance albeit that a Fourier approximation of TVG from the GRACE satellites is more realistic than a polynomial approximation. A difference of approximately 0.65 cm is achieved between our best solution (TVG-F) and the CNES POE-F orbits as we find them on the ESA cal/val server. The geographic mapping of the radial orbit difference as an average over the full CryoSat-2 period shows a north south banded structure where the mapped radial difference has an standard deviation of typically less than 1 cm on 1x1 degree grid cells.

We demonstrate a correlation between the evolution of the β angle and the sine and cosine components of the along track empirical acceleration model. Because of this correlation we recommend to investigate the tuning of the CNES solar radiation pressure model or similar alternatives to better predict ahead in time an empirical acceleration signal.

Declaration of Competing Interest

The authors declare that they have no known competing financial interests or personal relationships that could have appeared to influence the work reported in this paper.

Acknowledgements

Results obtained within ESA/ESRIN contract 4000112740 are used in this paper. We thank three reviewers for their suggestions that improved this paper.

References

Altamimi, Z., Rebischung, P., Collilieux, X., Métvier, L., Chanard, K., 2023. ITRF2020: an augmented reference frame refining the modeling of nonlinear station motions. J. Geodesy 97, 47. https://doi.org/10.1007/s00190-023-01738-w.

Bandikova, T., McCullough, C., Kruizinga, G.L., Save, H., Christophe, B., 2019. GRACE accelerometer data transplant. Adv. Space Res. 64 (3), 623–644. https://doi.org/10.1016/j.asr.2019.05.021.

Bruinsma, S., Boniface, C., 2021. The operational and research DTM-2020 thermosphere models. J. Space Weather Climate 11. https://doi.org/10.1051/swsc/2021032.

Chalmers, 2023. Chalmers university website ocean loading calculator, last access: 11-Oct-2023 http://holt.oso.chalmers.se/loading/.

Dobslaw, H., Bergmann-Wolf, I., Dill, R., Poropat, L., Thomas, M., Dahle, C., Esselborn, S., König, R., Flechtner, F., 2017. A new high-resolution model of non-tidal atmosphere and ocean mass variability for de-aliasing of satellite gravity observations: AOD1B RL06. Geophys. J. Int. 211 (1), 263–269. https://doi.org/10.1093/gji/ggx302.

Couhert et al., 2017. Next GDR-F POD Standards, IDS AWG meeting, UCL London UK, the presentation is available on the IDS website. https://ids-doris.org/images/documents/report/AWG201705/IDSAWG201705-Couhert-GDR-F.pdf

Donlon C.J., Cullen R., Giulicchi L., Vuilleumier P., Francis C.R., Kuschnerus M., Simpson W., Bouridah A., Caleno M., Bertoni R., Rancaño J., Pourier E., Hyslop A., Mulcahy J., Knockaert R., Hunter C., Webb A., Fornari M., Vaze P., Brown S., Willis J., Desai S., Desjonqueres J.-D., Scharroo R., Martin-Puig C., Leuliette E., Egido A., Smith W.H.F., Bonnefond P., Le Gac S., Picot N., Tavenrier G., 2021. The Copernicus Sentinel-6 mission: Enhanced continuity of satellite sea level measurements from space (2021) Remote Sensing of Environment, 258, art. no. 112395. DOI: 10.1016/j.rse.2021.112395.

Doornbos, E., 2012. Thermospheric Density and Wind Determination from Satellite Dynamics. Springer-Verlag, Berlin Heidelberg. https://doi.org/10.1007/978-3-642-25129-0.

Emmert, J.T., Jones, M., Siskind, D.E., Drob, D.P., Picone, J.M., Stevens, M.H., et al., 2022. NRLMSIS 2.1: An empirical model of nitric oxide incorporated into MSIS. J. Geophys. Res.: Space Phys. 127. https://doi.org/10.1029/2022JA030896.

Förste C, Bruinsma S., Abrykosov O., Rudenko S. Lemoine J.M., Marty J.C., Neumayer K.H., Biancale R., 2016. EIGEN-6S4 A time-variable satellite-only gravity field model to d/o 300 based on LAGEOS, GRACE and GOCE data from the collaboration of GFZ Potsdam and GRGS Toulouse. V. 2.0. GFZ Data Services. DOI: 10.5880/icgem.2016.008.

Hedin, A.E., 1987. MSIS-86 thermospheric model. J. Geophys. Res., Space Phys. 92 (A5), 4649–4662. https://doi.org/10.1029/JA092iA05p04649.

IDS, 2023a. International DORIS Service, last accessed 2-Nov-2023, http://www.ids-doris.org.

IDS, 2023b. International DORIS Service, Satellite tracks and visibility circles, last accessed 2-Nov-2023, https://ids-doris.org/doris-system/tracking-network/maps.html.

IERS, 2023a. International Earth Rotation Service, EOP 20 C04 series, IERS website data products EOP section, last accessed 2-Nov-2023, [link]

IERS, 2023b. International Earth Rotation Service, ITRF data products, IERS website data products ITRF section, last accessed 2-Nov-2023, [link]

ILRS, 2023. International Laser Ranging Service Website, SLR data, last accessed 2-Nov-2023, ILRS website Data and Products

Jayles C, Chauveau JP, Auriol A., 2015. DORIS/DIODE: Real-Time Orbit Determination Performance on Board SARAL/Altika, Marine Geodesy, Vol. 38, Issue sup1: The SARAL/Altika Satellite Altimeter Mission doi:10.1080/01490419.2015.1015695.

Khan, Shfaqat A. and Choi, Youngmin and Morlighem, Mathieu and Rignot, Eric and Helm, Veit and Humbert, Angelika, Mouginot, Jérémie, Millan, Romain, Kjær, Kurt H., Bjørk, Anders A., 2022. Extensive inland thinning and speed-up of Northeast Greenland Ice Stream Nature 611, 727–732 (2022). DOI: 10.1038/s41586-022-05301-z.

Knocke, P.C., Ries, J.C., Tapley, B.D., 1988. Earth radiation pressure effects on satellites. Proceedings of AIAA/AAS Astrodynamics Conference, 577–587. https://doi.org/10.2514/6.1988-4292.

König, R., Reinhold, A., Dobslaw, H., Esselborn, S., Neumayer, K.H., Dill, R., Michalak, A., 2021. On the effect of non-tidal atmospheric and oceanic loading on the orbits of the altimetry satellites ENVISAT, Jason-1 and Jason-2. Adv. Space Res. 68, 1048–1058. https://doi.org/10.1016/j.asr.2020.05.047.

Kornfeld, R.P., Arnold, B.W., Gross, M.A., Dahya, N.T., Klipstein, W. M., Gath, P.F., Bettadpur, S., 2019. GRACE-FO: the gravity recovery and climate experiment follow-on mission. J. Spacecr. Rock. 56 (3), 931–951. https://doi.org/10.2514/1.A34326.c1.

Lemoine FG, Kenyon SC, Factor JK, Trimmer RG, Pavlis NK, Chinn DS, Cox CM, Klosko SM, Luthcke SB, Torrence MH, Wang YM, Williamson RG, Pavlis EC, Rapp RH and Olson TR., 1998. The Development of the Joint NASA GSFC and NIMA Geopotential Model EGM96, NASA Goddard Space Flight Center, Greenbelt, Maryland, 20771 USA, July 1998. NASA/TP-1998-206861.

Loomis, B.D., Rachlin, K.E., Luthcke, S.B., 2019. Improved Earth oblateness rate reveals increased ice sheet losses and mass-driven sea level rise. Geophys. Res. Lett. 46, 6910–6917. https://doi.org/10.1029/2019GL082929.

Loomis, B.D., Rachlin, K.E., Wiese, D.N., Landerer, F.W., Luthcke, S. B., 2020. Replacing GRACE/GRACE-FO with satellite laser ranging: Impacts on Antarctic Ice Sheet mass change. Geophys. Res. Lett. 47. https://doi.org/10.1029/2019GL085488, e2019GL085488.

Luceri, V. et al., 2022. Systematic Errors in SLR Data Modeled in ITRF2020, UAW2022 Workshop 10.5281/zenodo.7243913.

Lyard, F.H., Allain, D.J., Cancet, M., Carrère, L., 2021. Picot N (2021) FES2014 global ocean tide atlas: design and performance. Ocean Sci. 17, 615–649. https://doi.org/10.5194/os-17-615-2021.

Moreaux, G., Willis, P., Lemoine, F.G., Zelensky, N.P., Couhert, A., Lakbir, H.A., Ferrage, P., 2019. DPOD2014: A new DORIS extension of ITRF2014 for precise orbit determination. Adv. Space Res. 63 (1), 118–138. https://doi.org/10.1016/j.asr.2018.08.043, ISSN 0273-1177.

Moreaux, G., Lemoine, F.G., Capdeville, H., Otten, M., Štěpánek, P., Saunier, J., Ferrage, P., 2023. The international DORIS service contribution to ITRF2020. Adv. Space Res. 72 (1), 65–91. https://doi.org/10.1016/j.asr.2022.07.012, ISSN 0273-1177.

Moreaux, G., Lemoine, F.G., Zelensky, N.P., Moyard, J., Couhert, A., 2023. DPOD2020: A DORIS extension of the ITRF2020 for precise orbit determination. Adv. Space Res., in press. https://doi.org/10.1016/j.asr.2023.10.006.

Naeije, M.C., Schrama, E., Scharroo, R., 2000. Radar Altimeter Database System project RADS. Int. Geosci. Remote Sensing Symp. (IGARSS) 2, 487–490. https://doi.org/10.1109/IGARSS.2000.861605.

Pavlis D.E., Poulouse S., McCarthy J.J., 2006. GEODYN Operations Manual (2006) Contractor report, SGT Inc, Greenbelt, MD.

Pearlman, M.R., Noll, C.E., et al., 2019. The ILRS: approaching 20 years and planning for the future. J. Geodesy 93 (11), 2161–2180. https://doi.org/10.1007/s00190-019-01241-1.

PODAAC, (2022) Distributed Active Archive Center, last accessed 2-Nov-2023 https://podaac.jpl.nasa.gov/cloud-datasets/dataaccess

Noll, C.E., Ricklefs, R., et al., 2019. Information resources supporting scientific research for the international laser ranging service. J. Geodesy 93 (11), 2211–2225. https://doi.org/10.1007/s00190-018-1207-2.

Peter Heike, Meyer Ulrich, Lasser Martin, Jäggi Adrian, 2022. COST-G, Time-variable gravity, Precise orbit determination, Low Earth Orbiter, Altimetry, Copernicus, Advances in Space Research, Number 12, pages 4155–4168, Volume 69. DOI: 10.1016/j.asr.2022.04.005.

Petit, G., Luzum, B. (Eds.), 2010. IERS Conventions, Technical Note No. 36, IERS Conventions Centre. https://www.iers.org/IERS/EN/Publications/TechnicalNotes/tn36.html.

Picot, N., Marechal, C., Couhert, A., et al., 2018. Jason-3 products handbook. SALP-MU-M-OP-16118-CN 1 (5), 28–31 https://www.ncei.noaa.gov/sites/default/files/2021-01/Jason-3%20Products%20Handbook.pdf.

Press, W.H., Flannery, B.P., Teukolsky, S.A., Vetterling, W.T., 1989. Numerical Recipes. Cambridge University Press, The Art of Scientific Computing.

Rapp, R.H., 1977. The relationship between mean anomaly block sizes and spherical harmonic representations. J. Geophys. Res. Vol. 82 (No. 33). https://doi.org/10.1029/JB082i033p05360.

Saunier, J., 2023. The DORIS network: advances achieved in the last fifteen years. Adv. Space Res. 72 (1), 3–22. https://doi.org/10.1016/j.asr.2022.07.016.

Schrama E. (2018) Precision orbit determination performance for CryoSat-2, Advances in Space Research, Volume 61, Issue 1, Pages 235-247, ISSN 0273-1177, doi.org/10.1016/j.asr.2017.11.001

Tapley, B.D., Bettadpur, S., Watkins, M., Reigber, C., 2004. The gravity recovery and climate experiment: Mission overview and early results. Geophys. Res. Lett. 31, L09607. https://doi.org/10.1029/2004GL019920.

Tapping, K.F., 2013. The 10.7 cm solar radio flux (F10.7). Space Weather 11 (7), 394–406. https://doi.org/10.1002/swe.20064.

Willis, P., Haines, B., Berthias, J.-P., Sengenes, P., Le Mouël, J.-L., 2004. Comportement de l'oscillateur DORIS/Jason au passage de l'anomalie sud-atlantique. C.R. Geosci. 336 (9), 839–846. https://doi.org/10.1016/j.crte.2004.01.004, ISSN 1631-0713.

Willis, P., Lemoine, F.G., Moreaux, G., Soudarin, L., Ferrage, P., Ries, J., Otten, M., Saunier, J., Noll, C., Biancale, R., Luzum, B., 2016. In: Rizos, Chris, Willis, Pascal (Eds.), The International DORIS Service (IDS): Recent Developments in Preparation for ITRF2013, Springer International Publishing, IAG 150 Years, pp. 631–640. https://doi.org/10.1007/1345_2015_164.

Wingham, D.J., Francis, C.R., Baker, S., Bouzinac, C., Brockley, D., Cullen, R., de Chateneau-Thierry, P., Laxon, S.W., Mallow, U., Mavrocordatos, C., Phalippou, L., Ratier, G., Rey, L., Rostan, F., Viau, P., Wallis, D.W., 2006. CryoSat: A mission to determine the fluctuations in the Earth's land and marine ice fields. Adv. Space Res. 37, 841–871. https://doi.org/10.1016/j.asr.2005.07.027.

Space Weather Prediction Center (2023), last accessed 6-Nov-2023. https://www.swpc.noaa.gov/.